DOI: 10.1002/ejic.201000491

Polyoxometalate-Based Metal-Organic Frameworks as Heterogeneous Catalysts for Selective Oxidation of Ethylbenzene

Fan Yu,[a] Pei-Qing Zheng,[a] Yu-Xiang Long,[a] Yan-Ping Ren,[a] Xiang-Jian Kong,*[a] La-Sheng Long,*[a] You-Zhu Yuan,*[a] Rong-Bin Huang,[a] and Lan-Sun Zheng[a]

Keywords: Polyoxometalates / Metal-organic frameworks / Heterogeneous catalysis / Oxidation

The catalytic properties of four polyoxometalate (POM)-based metal-organic frameworks, $\{[Cu_2(4,4'\text{-bipy})_4(H_2O)_4](SiW_{12}O_{40})(H_2O)_{18}\}_n$ (**1**), $\{[Cu_2(4,4'\text{-bipy})_4(H_2O)_4](SiW_{12}O_{40})(4,4'\text{-bipy})_2(H_2O)_4\}_n$ (**2**), $\{[Cu_2(4,4'\text{-bipy})_4(H_2O)_4](PW_{12}O_{40})(H_2O)_{18}\}_n$ (**3**), and $\{[Cu_2(4,4'\text{-bipy})_4(H_2O)_4](PMo_{12}O_{40})(H_2O)_{18}\}_n$ (**4**) (bipy = bipyridine), for the oxidation of ethylbenzene were investigated. Complexes **1**–**4**, which feature 3D frameworks formed through static incorporation between distinct Keggin POMs and the same voids in the 2D network of $[Cu_2(4,4'\text{-bipy})_4(H_2O)_4]_n^{4n+}$, show the distinct conversion and selectivity for the oxidation of ethylbenzene. Investigation into the difference in the catalytic activity of **1**–**4** reveals that the oxidation of the substrate was performed in the pore of the framework and that the valence of the metal ion in the polyoxometalates significantly affects the catalytic activity of the 3D framework.

Introduction

Owing to various advantages,[1] polyoxometalates (POMs) have been applied to several large-scale commercial processes and are regarded as promising green catalysts.[1–4] However, the difficulty in controlling the pore size, the aggregation of POMs in preparation of the catalyst, and the limited variation in chemical formulation and functionality often limit their applications.[4] One of the approaches to solve the problems is to use transition metals, organic ligands, and POMs to assemble POM-based metal-organic frameworks.[5–11] Although the approach has successfully solved the problem of aggregation of POMs in the catalytic process and offers great potential for chemical and structural diversity, investigation of the catalytic properties of these kinds of materials is rather limited.[2b,12–14]

In previous works, we have developed an approach for the construction of POM-based metal-organic frameworks through direct static incorporation between POMs and the voids in the 2D network.[15] In comparison with that of covalently linking the metal-organic unit and POMs into a 3D structure, the approach of constructing POM-based metal-organic frameworks through direct static incorporation does not only provide a convenient synthetic route to porous POMs-based materials; the pore of the material also exhibits a unique flexibility.[15] By selecting Keggin-type $SiW_{12}O_{40}^{4-}$ and a four-connected 2D network of $[Cu(4,4'\text{-bipy})_2(H_2O)_2]_n^{2n+}$ (bipy = bipyridine), we have reported two complexes, $\{[Cu_2(4,4'\text{-bipy})_4(H_2O)_4](SiW_{12}O_{40})(H_2O)_{18}\}_n$ (**1**) and $\{[Cu_2(4,4'\text{-bipy})_4(H_2O)_4](SiW_{12}O_{40})(4,4'\text{-bipy})_2(H_2O)_4\}_n$ (**2**).[15] As a continuation of our work in this respect, we report here the synthesis and structures of $\{[Cu_2(4,4'\text{-bipy})_4(H_2O)_4](PW_{12}O_{40})(H_2O)_{18}\}_n$ (**3**) and $\{[Cu_2(4,4'\text{-bipy})_4(H_2O)_4](PMo_{12}O_{40})(H_2O)_{18}\}_n$ (**4**), which are constructed of different Keggin-type POMs ($PW_{12}O_{40}^{4-}$ for **3** and $PMo_{12}O_{40}^{4-}$ for **4**) and the same voids in a 2D network. Most importantly, the catalytic properties of complexes **1**–**4** for the oxidation of ethylbenzene were also investigated. We hope, based on the investigation of structure–activity correlations, to understand the key factors that influence their catalytic properties so as to provide some hints for the design of highly efficient catalysts in the future.

Results and Discussion

Description of Crystal Structures of Catalysts 3 and 4

The structure of **3** is shown in Figure 1, which can be viewed as an adjacent four-connected 2D structure of $[Cu(4,4'\text{-bipy})_2(H_2O)_2]_n^{2n+}$ (Figure 2) connected through the direct static incorporation between the $PW_{12}O_{40}^{4-}$ anion and the 2D structure. The remaining void space of the metal-organic framework is occupied by water molecules. The metal-organic framework of **4** is very similar to that of **3**. Structurally, **4** can be viewed as the $PW_{12}O_{40}^{4-}$ anion in **3** replaced by $PMo_{12}O_{40}^{4-}$. Thus the four POM-based metal-organic frameworks are structural isomers of each other, and the structure of **1** can be viewed as the $PMo_{12}O_{40}^{4-}$

[a] State Key Laboratory of Physical Chemistry of Solid Surface and Department of Chemistry, College of Chemistry and Chemical Engineering, Xiamen University,
Xiamen 361005, P. R. China
Fax: +86-592-218-3047
E-mail: xjkong@xmu.edu.cn
lslong@xmu.edu.cn
yzyuan@xmu.edu.cn

Supporting information for this article is available on the WWW under http://dx.doi.org/10.1002/ejic.201000491.

anion in **3** replaced by the $SiW_{12}O_{40}^{4-}$ anion, whereas the structure of **2** can be viewed as the $PW_{12}O_{40}^{4-}$ anion and part of guest water molecules in **3** replaced by the $SiW_{12}O_{40}^{4-}$ anion and 4,4′-bipy guest molecules. In the structures of **3** and **4**, the charge of the $PW_{12}O_{40}^{4-}$ and $PMo_{12}O_{40}^{4-}$ anions is –4, which is due to the valence of one W or Mo being +5; this is demonstrated from the X-ray photoelectron spectroscopy (XPS) spectra and magnetic measurements of **3** and **4**. As shown in Figure S1a in the Supporting Information, the four overlapped peaks at 34.87, 35.23, 37.05, and 37.41 eV are ascribed to W^{5+} ($4f_{7/2}$), W^{6+} ($4f_{7/2}$), W^{5+} ($4f_{5/2}$), and W^{6+} ($4f_{5/2}$), respectively, whereas the four overlapped peaks at 231.16, 232.36, 234.29, and 235.49 eV are ascribed to Mo^{5+} ($3d_{5/2}$), Mo^{6+} ($3d_{5/2}$), Mo^{5+} ($3d_{3/2}$), and Mo^{6+} ($3d_{3/2}$), respectively (Figure S1b). The existence of one W^{5+} in the POMs in **3** is further confirmed from the experimental and simulated XPS spectra of **3**, in which the ratio of W^{6+} to W^{5+} equals 11:1 based on the peak area obtained from the simulated XPS spectra.[16] Similarly, the only Mo^{5+} is obtained from the simulated XPS spectra of **4**. The reduction of the POM anions was often observed in the reaction of a nitrogen-containing ligand with a POM anion under hydrothermal conditions.[17] The oxidation-state change of W (or Mo) atoms from a reactant W^{VI} (or Mo^{V}) to a resultant W^{V} (or Mo^{V}) in complex **3** (or **4**) is probably associated with the 4,4′-bipy ligand.

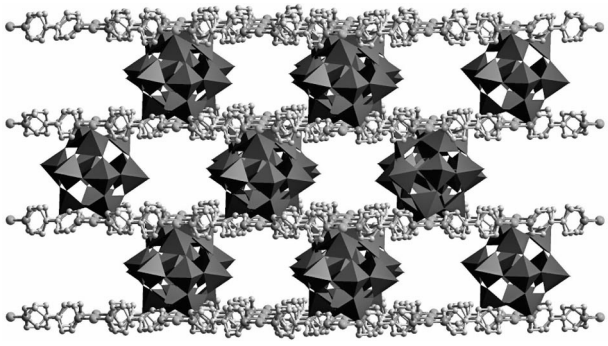

Figure 1. Polyhedron plot showing the 3D structure of **3**.

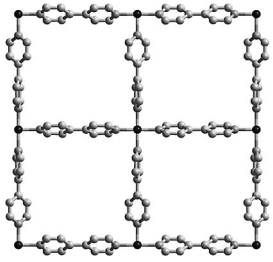

Figure 2. Ball-and-stick plot showing the structure 4^4 network of $[Cu(4,4'\text{-bipy})_2(H_2O)_2]_n^{2n+}$ in **3**.

To validate one W^{5+} in the POMs in **3** and one Mo^{5+} in **4**, the variable-temperature magnetic-susceptibility data for **1**–**4** were recorded between 2 and 300 K under a magnetic field of 10 kOe. The plots of $\chi_M T$ versus T are shown in Figure 3a. At room temperature, for **1**, the $\chi_M T$ value is equal to 0.73 emu K mol^{-1}, which closely approximates the predicted spin-only value (0.75 emu K mol^{-1}) for two Cu^{II} (S = ½, g = 2.0) centers. As the temperature is lowered, the $\chi_M T$ values remain constant at around 0.72 emu K mol^{-1} down to 20 K. This suggests the presence of paramagnetic properties of the Cu^{II} ion in accordance with the other $Cu(4,4\text{-bipy})_2$ compounds in which the copper ions are supposed to have only weak interactions due to long Cu···Cu distances.[18] Below 20 K, the $\chi_M T$ decreases abruptly down to 2 K (0.45 emu K mol^{-1}). This might be caused by the zero-field splitting at low temperature. For **2**, the same $\chi_M T$ versus T plots are exhibited as for **1**; the $\chi_M T$ value is 0.73 emu K mol^{-1} at 300 K, remains constant around 0.71 emu K mol^{-1} until reaching 16 K, and decreases to 0.47 emu K mol^{-1} at 2 K. But for **3**, the $\chi_M T$ value is 1.16 emu K mol^{-1}. This corresponds to the calculated value 1.125 emu K mol^{-1} of two Cu^{II} (S = ½, g = 2.0) and one W^{V} (S = ½, g = 2.0) centers, which confirms the presence of two Cu^{II} and one W^{V} ion existing in the crystal structure. Similar characteristics of paramagnetic behavior are exhibited from 300 to 20 K, which is indicated by very weak interactions between Cu···Cu and Cu···W due to long interaction distances. The $\chi_M T$ values decrease respectively to 0.92 emu K mol^{-1} at 2 K. For **4**, the same characteristics of paramagnetic behavior are exhibited as for **3**: the $\chi_M T$ value is 1.11 emu K mol^{-1} at 300 K, which is in accordance with the calculated value (1.125 emu K mol^{-1}) of two Cu^{II} (S = ½, g = 2.0) centers and one Mo^{V} (S = ½, g = 2.0) center per Cu_2Mo unit.

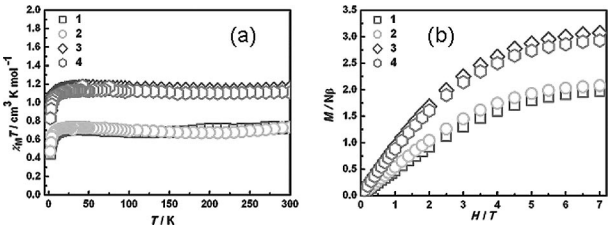

Figure 3. (a) The plots of $\chi_M T$ versus T for **1**–**4**; (b) the plots of the field dependence of magnetization for **1**–**4**.

The field dependence of magnetizations for **1**–**4** measured at 2 K is shown in Figure 3 (b). For **1** and **2**, it can be seen that the observed magnetization (M) is in good accordance with the values predicted from the Brillouin function for two Cu^{II} ions with g = 2.0 [$M = 2 \times (2 \times ½)$]. Similar to **1** and **2**, the magnetization per Cu_2W or Cu_2Mo of **3** and **4** is also in line with the values predicted from the Brillouin function for two Cu^{II} and one W^{V} or Mo^{V} ions with g = 2.0 [$M = 2 \times (2 \times ½ + ½)$]. All of the magnetizations measured at 2 K are consistent with the results deduced from the magnetic-susceptibility data.

The accessible porosity in **1** to **4** for a guest molecule calculated through the PLATON program[19] is 3089.8 Å^3 mol^{-1} (35.3%) for **1**, 2681.5 Å^3 mol^{-1} (31.5%) for **2**, 3065.7 Å^3 mol^{-1} (34.6%) for **3**, and 2991.5 Å^3 mol^{-1} (33.9%) for **4**. However, it is difficult to measure the surface area and pore size of the related metal-organic frameworks

due to the removal of the guest, thereby resulting in the layer distance in these metal-organic frameworks being significantly shortened.[15]

Heterogeneous Catalytic Activity of 1

Catalytic Test

A probe reaction of the oxidation of ethylbenzene was carried out to investigate the oxidative catalytic activity of **1**–**4** (Scheme 1). To optimize the product yield and selectivity, complex **1** and *tert*-butyl hydroperoxide (TBHP) were selected as the catalyst and oxidant (Table 1), respectively, to investigate the influences of different reaction parameters (i.e., reaction temperature, reaction solvent, reaction time, catalyst amount, and TBHP concentration) on the oxidation of ethylbenzene. Table 1 shows the results about the influences of different parameters on the performance of **1** toward the oxidation of ethylbenzene.

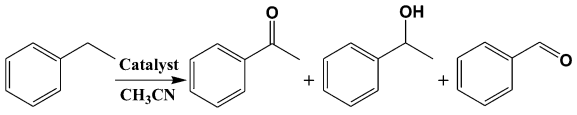

Scheme 1. Oxidation of ethylbenzene to acetophenone.

Table 1. Selective oxidation of ethylbenzene by **1** using TBHP oxidant.[a]

Entry	Solvent	*T* [K]	*t* [h]	TBHP/ substrate	Conversion[b] [%]	Selectivity[b] [%]
1[a]	CH_3CN	343	12	2	56.8	88.1
2[a]	CH_3OH	343	12	2	3.1	28.7
3[a]	CH_3COCH_3	343	12	2	8.7	38.7
4[a]	CH_3CN	313	12	2	9.0	65.8
5[a]	CH_3CN	323	12	2	28.5	71.0
6[a]	CH_3CN	333	12	2	35.0	76.2
7[a]	CH_3CN	353	12	2	54.4	75.9
8[a]	CH_3CN	343	6	2	43.7	79.1
9[a]	CH_3CN	343	8	2	49.2	82.4
10[a]	CH_3CN	343	10	2	55.7	85.2
11[a]	CH_3CN	343	18	2	59.7	88.6
12[a]	CH_3CN	343	24	2	62.3	86.2
13[a]	CH_3CN	343	12	0	0	0
14[a]	CH_3CN	343	12	1	37.2	84.6
15[a]	CH_3CN	343	12	3	57.5	84.5
16[c]	CH_3CN	343	12	2	6.6	0
17[d]	CH_3CN	343	12	2	40.1	77.1
18[e]	CH_3CN	343	12	2	44.0	84.8
19[f]	CH_3CN	343	12	2	56.6	85.2

[a] Ethylbenzene (0.3 mL, 2.44 mmol) and catalyst (0.01 mmol) in CH_3CN (8 mL). [b] The average conversion of two runs based on GC results. The reaction mixture was analyzed twice, before and after treatment with PPh_3. No differences from each other were obtained. Ethylbenzene conversion [%] was defined as: conv. = $(n_{ap} + n_{ba} + n_{panol} + n_{other}) \times 100/n_{eb0}$; acetophenone selectivity [%] was defined as: selec. = $n_{ap} \times 100/(n_{ap} + n_{ba} + n_{panol} + n_{other})$ [n_{eb0}: the initial molarity of ethylbenzene; eb = ethylbenzene; ap = acetophenone; ba = benzaldehyde; panol = 1-phenylethanol; other = other products (mainly benzoic acid)]. [c] No catalyst exits in the reaction. [d] Catalyst (2.5×10^{-3} mmol). [e] Catalyst (0.005 mmol). [f] Catalyst (0.015 mmol).

Generally, the nature of the solvent plays a very important role in the catalytic reactions carried out in the liquid phase.[20–21] On account of **1** being completely insoluble in organic solvents of methanol, acetonitrile, and acetone, the reaction with **1** as the catalyst was performed at 343 K in the presence of methanol, acetonitrile, and acetone, respectively. As shown in entries 1–3 in Table 1, the conversion (and selectivity) for the oxidation of ethylbenzene to acetophenone conducted in methanol, acetone, and acetonitrile was 3.1 (28.7%), 8.7 (38.7%), and 56.8% (88.1%), respectively. This result indicates that acetonitrile is the best solvent for the reaction.

Since the acetonitrile is the best solvent for the reaction, the effect of reaction temperatures on the oxidation of ethylbenzene with **1** as the catalyst was investigated in the presence of acetonitrile. As shown in entries 1 and 4–6 in Table 1, both the conversion and selectivity for the oxidation of ethylbenzene to acetophenone increase linearly in the temperature range 313 to 343 K. However, with a further increase in temperature, the conversion and selectivity for the oxidation of ethylbenzene to acetophenone decrease (entry 7). The lower conversion at 353 K might be attributed to the decomposition of TBHP[22] as well as the higher temperature that results in further oxidation of acetophenone to form overoxidized byproducts.[23]

When extending the reaction time from 6 to 24 h (Table 1, entries 1 and 8–12), both the conversion and acetophenone selectivity increased linearly and reached almost saturation after 12 h of reaction. With a further increase in reaction time, the reaction conversion increases slightly, whereas the selectivity of acetophenone decreases slightly. There was no significant increase in the conversion and selectivity when extending the reaction time up to 24 h. This may be related to the reaction reaching saturation by 12 h, which suggests that 12 h is sufficient to afford optimized yields and selectivity.

The effect of TBHP amount on oxidation of ethylbenzene is presented in entries 1 and 13–15 of Table 1. In the absence of any TBHP, oxidation of ethylbenzene to acetophenone was not observed. By varying the ratio of TBHP to ethylbenzene from 1:1 to 2:1, the conversion of ethylbenzene to acetophenone increased from 37.2 to 56.8%, and no TBHP was detected in the reaction mixture when the ratio was 1:1. However, the conversion of ethylbenzene to acetophenone slightly decreased when the ratio of TBHP to ethylbenzene was increased to 3:1, thus suggesting that the best ratio of TBHP to ethylbenzene for the conversion of ethylbenzene to acetophenone is 2:1.

The effect of catalyst amount on oxidation of ethylbenzene is presented in entries 1 and 16–19 of Table 1. In the absence of any catalyst, the oxidation of ethylbenzene is negligible (conversion of ethylbenzene is only 6.6%) after the reaction has been performed at 343 K for 12 h. With an increase in the amount of catalyst, the ethylbenzene conversion increases and reached a maximum of 56.8% when the amount of catalyst reached 0.01 mmol. However, the conversion slightly decreased and acetophenone selectivity displayed a decreasing pattern when the amount of catalyst

increased to 0.015 mmol. This result suggests that the best amount of catalyst for the oxidation of ethylbenzene to acetophenone is 0.01 mmol.

Heterogeneous Catalytic Activity of 1 and Its Recyclel Reuse

In the study of heterogeneous catalysts for liquid–solid reactions, whether the reaction activity derives from the insoluble solid catalyst or from a small quantity of dissolved catalyst is of key importance for the assessment of the catalytic properties.[2b] Thus, the amount of metal ions in the reaction filtrate was tested by atomic absorption spectra. No copper species (<0.1 ppm) were detected in the filtrate, thereby indicating that the catalytic process is truly heterogeneous. Consistently, when **1** was used in the catalytic reaction, not only was the filtrate catalytically inactive for the oxidation reaction (Figure S2 in the Supporting Information), but also no change occurred in the X-ray powder diffractometry (XRPD) patterns before and after the catalyst was used for the catalytic reaction (Figure S3 in the Supporting Information). More importantly, when the catalyst was reused for the subsequent oxidation reaction, the conversion of ethylbenzene kept the original conversion, and there is no significant loss of activity under similar conditions even after three consecutive cycles (Figure S4 in the Supporting Information).

Catalytic Activities of 1 to 4

Since the oxidation of ethylbenzene originates from the catalyst, the catalytic activity of **1**–**4** was investigated under the optimized reaction conditions [i.e., ethylbenzene (0.3 mL, 2.44 mmol), catalyst (0.01 mmol), and 70% TBHP (0.754 mL, 4.88 mmol), acetonitrile (8.0 mL), 70 °C, and 12 h] so as to reveal the relationship between structure and catalytic properties. In addition, the catalytic activity of corresponding POMs was also investigated under identical conditions for comparison. As shown in Table 2, the catalytic activity of **1**–**4** toward the oxidation of ethylbenzene is significantly higher than those of corresponding POMs, comparable to the catalytic activity of the reported [Cu([H]$_2$-N$_4$)](ClO$_4$) and Co-HMS (100).[24a–b] The catalytic activity of **1**–**4** for the oxidation of ethylbenzene follows the order **1** > **3** ≈ **4** > **2**. It was noted that, in addition to the heterogeneous catalyst of $Na_4SiW_{12}O_{40}$, $Na_3PW_{12}O_{40}$, and $Na_3PMo_{12}O_{40}$, the catalytic activity for the homogeneous catalyst of $(Bu_4N)_4SiW_{12}O_{40}$ and 4,4-bipy is also significantly poorer than that of **1**–**4**. This result indicates that the catalytic activity for **1**–**4** is likely enhanced by copper incorporated in the POM, which would be consistent with the fact that the multinuclear copper complexes have the requisite catalytic activity for C–H oxidation.[24] Based on the structural analysis of **1**–**4**, the catalytic activity of **1** is higher than that of **3** and **4**. This can be attributed to fact that the valence of one metal ion of POMs in **3** and **4** is +5, since the reduced tungsten and molybdenum atom would change the electric charges of the polyoxometalate and lead to the lower oxidation.[25]

Table 2. The effect of different catalysts on ethylbenzene oxidation.[a]

Catalyst	*T* [K]	Solvent	Conversion [%]	Selectivity [%]
1	343	CH_3CN	56.8	88.1
2	343	CH_3CN	37.9	80.1
3	343	CH_3CN	44.5	82.2
4	343	CH_3CN	45.1	86.5
$(Bu_4N)_4SiW_{12}O_{40}$	343	CH_3CN	35.4	79.1
$Na_4SiW_{12}O_{40}$	343	CH_3CN	27.5	76.4
$Na_3PW_{12}O_{40}$	343	CH_3CN	11.4	65.6
$Na_3PMo_{12}O_{40}$	343	CH_3CN	28.6	76.0
4,4′-bipy[b]	343	CH_3CN	10.8	–
Blank	343	CH_3CN	6.6	–

[a] Reaction conditions: catalyst (0.01 mmol), ethylbenzene(0.3 mL, 2.44 mmol), TBHP (0.754 mL, 4.88 mmol), CH_3CN (8.0 mL), reaction time 12 h. [b] Catalyst (0.04 mmol).

It was mentioned that the valence of POM influencing the catalytic properties of the framework implies that the POM in the framework plays a key role in the catalytic process. Notably, although the 3D framework of **1** is very similar to that of **2**, both the conversion and selectivity of oxidation of ethylbenzene for **1** are significantly higher than those of **2**. This result indicates that guest molecule of 4,4′-bipy has a significant influence on the catalytic properties. Given that the guest molecule of 4,4′-bipy is located in the pore of the framework, the significant difference in the catalytic activity between **1** and **2** suggests that the oxidation reaction is performed in the pore of the framework. This is understandable from their structures, since the guest molecule of 4,4′-bipy in **2** could effectively prevent the substrate from entering its pore. To confirm that the difference in catalytic activity between **1** and **2** is related to the guest molecule of 4,4′-bipy in the pore, thereby preventing the substrate from entering the pore, a time-dependent oxidation reaction of 1-phenylethanol for **1** and **2** was carried out (Scheme 2). As shown in Figure 4, in contrast to the linear increase over the whole reaction time for **1**, the conversion rate of the oxidation reaction for **2** is almost unchanged when the reaction was performed within 5 h, and very close to that of **1** when the reaction time is longer than 5 h. These results indicate that the guest molecule of 4,4′-bipy in **2** remains in its pore at the beginning of the reaction and has been fully exchanged by the time the reaction exceeds 5 h, which was further confirmed by the XRPD patterns of **2** dipped in MeCN. As shown in Figure S5 in the Supporting Information, when **2** is dipped in MeCN for 1 h, its XRPD patterns show that part of the guest molecule of 4,4′-bipy is removed, whereas when **2** was dipped for about 5 h, its XRPD patterns revealed that the guest molecules of 4,4′-bipy in **2** are fully exchanged; fitting these patterns (see the Supporting Information) gives unit-cell

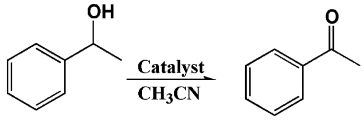

Scheme 2. Oxidation of 1-phenylethanol to acetophenone.

parameters of a = 17.823 Å, b = 22.146 Å, and c = 22.225 Å.[26] Unambiguously, the easier exchange of the molecule of 4,4′-bipy is attributed to the static interaction between the 2D network and the POMs, which is consistent with the result previously reported in zeolite-like metal-organic frameworks.[14j–m]

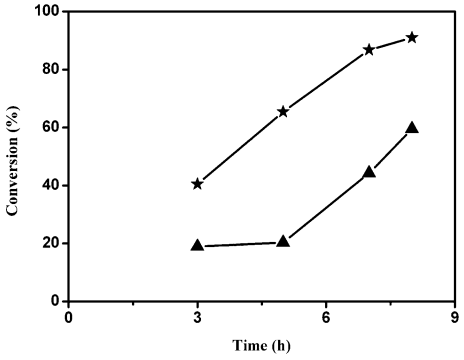

Figure 4. The effect of time on 1-phenylethanol oxidation with **1** and **2** as catalysts. (*) 1-Phenylethanol conversion [%] with **1** as catalyst; (▲) 1-phenylethanol conversion [%] with **2** as catalyst; reaction conditions: catalyst (0.01 mmol), 1-phenylethanol (0.2 mL, 1.65 mmol), TBHP (0.4 mL, 2.6 mmol), T = 333 K, CH_3CN (8.0 mL).

Conclusion

POM-based metal-organic frameworks represent an outstanding class of functional materials and are also considered to be green materials. In this work, we have reported the catalytic activity of four POM-based metal-organic frameworks toward the oxidation of ethylbenzene, as well as the optimized conditions for the catalytic reaction. Investigation on the structure–activity correlations reveals that the oxidation of the substrate occurred in the pore of the framework, and that the valence of the metal ion in the POMs significantly influences the catalytic of the 3D framework. Hence, the present work would be helpful for the rational design of new POM-based catalysts for other important organic transformations.

Experimental Section

Materials and Measurements: Ethylbenzene was repurified before use. TBHP (70%) was purchased commercially. Other reagents used in the work were all AR grade. Atomic absorption results were obtained with a Thermo Electron IRIS Intrepid II XSP. XPS studies of the complexes were performed with a Physical Electrons Quantum 2000 Scanning Esca Microprob spectrometer. XRPD was performed with a Panalytical X-Pert pro diffractometer with Cu-K_α radiation (λ = 0.15418 nm, 40.0 kV, 30.0 mA). The reaction products of oxidation were determined and analyzed with a GC-920 instrument with a capillary column (30 m × 0.25 mm); benzyl alcohol (analytical pure grade) was used as internal standard for GC measurements. Magnetic measurements were carried out with a Quantum Design MPMS XL-7 magnetometer working in the DC mode. The measurements were performed in the range of 2–300 K with a magnetic field of 10 kOe. The FTIR spectrum was recorded with a Nicolet AVATAR FTIR360 Spectrophotometer in the 4000–400 cm^{-1} range with pressed KBr pellets.

Synthesis of Catalysts 1 to 4: Complexes **1** and **2** were prepared as described previous work.[15] Complex **3** was prepared as follows: $Na_3PW_{12}O_{40}$ (1.18 g, 0.40 mmol), 4,4′-bipy (0.06 g, 0.4 mmol), and $Cu(NO_3)_2{\cdot}3H_2O$ (0.19 g, 0.8 mmol) were dissolved in distilled water (10 mL) with stirring at room temperature. When the pH value of the mixture was adjusted to about 6 with 1.0 mol L^{-1} NaOH, the cloudy solution was put into a 25 mL Teflon®-lined Parr autoclave and heated to 190 °C for 48 h, and then cooled to 100 °C at a rate of 5 °C h^{-1}. After remaining at 100 °C for 10 h, the mixture was cooled to room temperature at a rate of 5 °C h^{-1}. Blue crystals of **3** were obtained in 40% yield (based on 4,4′-bipy). $C_{40}H_{76}Cu_2N_8O_{62}PW_{12}$ (4025.32): calcd. C 11.90, H 1.88, N 2.78; found C 11.73, H 1.64, N 2.79. IR (KBr): $\tilde{\nu}$ = 3432 (s), 1611 (s), 1530 (w), 1491 (w), 1414 (m), 1214 (m), 1102 (w), 1061 (s), 954 (s), 881 (m), 810 (s), 748 (w), 518 (m) cm^{-1}. Complex **4** was prepared as follows: $H_3[PMo_{12}O_{40}]$ (0.73 g, 0.40 mmol), 4,4′-bipy (0.06 g, 0.4 mmol), $Cu(NO_3)_2{\cdot}3H_2O$ (0.19 g, 0.8 mmol), and anhydrous ethanol (1.0 mL) were dissolved in distilled water (12 mL) with stirring at room temperature. When the pH value of the mixture was adjusted to about 5 with 1.0 mol L^{-1} NaOH, the cloudy solution was put into a 25 mL Teflon®-lined Parr autoclave and heated to 165 °C for 24 h, and then cooled to 100 °C at a rate of 5 °C h^{-1}. After remaining at 100 °C for 10 h, the mixture was cooled to room temperature at a rate of 5 °C h^{-1}. Brown crystals of **4** were obtained in 13.1% yield (based on 4,4′-bipy). $C_{40}H_{76}Cu_2Mo_{12}N_8O_{62}P$ (2970.40): calcd. C 16.16, H 2.56, N 3.77; found C 16.64, H 2.26, N 3.87. IR (KBr): $\tilde{\nu}$ = 3435 (s), 2925 (m), 1615 (s), 1537 (w). 1460 (w), 1417 (m), 1384 (m), 1222 (m), 1055 (w), 946 (m), 906 (vs), 796 (vs), 534 (m) cm^{-1}.

X-ray Crystallography: The data for single-crystal X-ray structure determination were collected with a Bruker SMART Apex CCD diffractometer at 298 K for **3** and 173 K for **4**. Absorption corrections were applied using the multiscan program SADABS.[27] The structures were solved by direct methods, and the non-hydrogen atoms were refined anisotropically by the least-squares method on F^2 with the SHELXTL program.[28] The hydrogen atoms of the organic ligand were generated geometrically (C–H, 0.96 Å). All the guest water molecules in a unit were removed by SQUEEZE; 18 water molecules were determined by elemental analysis. Crystal data for **3**: orthorhombic; space group *Cccm*; a = 17.965(4) Å, b = 22.164(4) Å, c = 22.225(4) Å; V = 8849(3) $Å^3$; Z = 4; $\rho_{calcd.}$ = 3.021 g cm^{-3}; μ = 16.121 mm^{-1}; M_r = 4025.34; R_1(obsd.) = 0.0867; wR_2(all data) = 0.2231; GOF (F^2) = 1.025. Crystal data for **4**: orthorhombic; space group *Cccm*; a = 17.847(4) Å, b = 22.178(4) Å, c = 22.284(5) Å; V = 8820(3) $Å^3$; Z = 4; $\rho_{calcd.}$ = 2.237 g cm^{-3}; μ = 2.243 mm^{-1}; M_r = 2970.42; R_1(obsd.) = 0.0791; wR_2(all data) = 0.2101; GOF (F^2) = 1.032.

CCDC-705473 (for **3**) and -705474 (for **4**) contain the supplementary crystallographic data for this paper. These data can be obtained free of charge from The Cambridge Crystallographic Data Centre via www.ccdc.cam.ac.uk/data_request/cif.

Heterogeneous Oxidation of Ethylbenzene and 1-Phenylethanol: Oxidation reactions of ethylbenzene or 1-phenylethanol were carried out in a round-bottomed flask fitted with a water-cooled condenser by using 70 wt.-% aqueous *tert*-butyl hydroperoxide (TBHP) as oxidant. The reaction mixture was centrifuged to remove the catalyst and analyzed by gas chromatography with a flame-ionization detector (FID) and a capillary column (30 m × 0.25 mm). Assignments were made by comparison with authentic samples analyzed under the same condition.

Supporting Information (see also the footnote on the first page of this article): XPS spectra of **3** and **4**, XRD patterns of **1** and **2**, the catalytic result of recycling **1** three times, the IR spectra, and the simulation of space group and unit cell from XRPD patterns of **2** dipped in MeCN for 5 h.

Acknowledgments

We thank the National Natural Science Foundation of China (NSFC) (grant numbers 20825103, 90922031, and 20721001), the 973 Project from the Ministry of Science and Technology of China (MSTC) (grant 2007CB815304), and the Natural Science Foundation of Fujian Province (2009J01041).

[1] a) I. V. Kozhevnikov, *Chem. Rev.* **1998**, *98*, 171–198; b) A. Müller, S. Roy, *Coord. Chem. Rev.* **2003**, *245*, 153–166; c) N. Mizuno, M. Misono, *Chem. Rev.* **1998**, *98*, 199–218.

[2] a) T. Okuhara, N. Mizuno, M. Misono, *Adv. Catal.* **1996**, *41*, 113–252; b) J. T. Rhule, W. A. Neiwert, K. I. Hardcastle, B. T. Do, C. L. Hill, *J. Am. Chem. Soc.* **2001**, *123*, 12101–12102.

[3] a) N. Nojiri, M. Misono, *Appl. Catal.* **1993**, *93*, 103–122; b) M. Eddaoudi, D. B. Moler, H. Li, B. Chen, T. M. Reineke, M. O'Keeffe, O. M. Yaghi, *Acc. Chem. Res.* **2001**, *34*, 319–330; c) B. Moulton, M. J. Zaworotko, *Chem. Rev.* **2001**, *101*, 1629–1658; d) O. M. Yaghi, M. O'Keeffe, N. W. Ockwig, H. K. Chae, M. Eddaoudi, J. Kim, *Nature* **2003**, *423*, 705–714; e) D. Bradshaw, J. B. Claridge, E. J. Cussen, T. J. Prior, M. J. Rosseinsky, *Acc. Chem. Res.* **2005**, *38*, 273–282; f) C. L. Hill, *J. Mol. Catal. A* **2007**, *262*, 2–6.

[4] a) M. Misono, *Chem. Commun.* **2001**, 1141–1152; b) A. R. Gasper, J. A. F. Gamelas, D. V. Evtuguin, C. P. Neto, *Green Chem.* **2007**, *9*, 717–730.

[5] J. Y. Niu, M. L. Wei, J. P. Wang, D. B. Dang, *J. Mol. Struct.* **2003**, *655*, 171–178.

[6] A. Dolbeq, P. Mialane, L. Lisnard, J. Marrot, F. Sécheresse, *Chem. Eur. J.* **2003**, *9*, 2914–2920.

[7] L. M. Duan, C. L. Pan, J. Q. Xu, X. B. Cui, F. T. Xie, T. G. Wang, *Eur. J. Inorg. Chem.* **2003**, *14*, 2578–2581.

[8] M. Yuan, Y. G. Li, E. Wang, Y. Lu, C. W. Hu, N. H. Hu, H. Q. Jia, *J. Chem. Soc., Dalton Trans.* **2002**, 2916–2920.

[9] W. Yang, C. Lu, H. Zhuang, *J. Chem. Soc., Dalton Trans.* **2002**, 2879–2884.

[10] W. M. Bu, L. Ye, G. Y. Yang, J. S. Gao, Y. G. Fan, M. C. Shao, J. Q. Xu, *Inorg. Chem. Commun.* **2001**, *4*, 1–4.

[11] a) G. Luan, Y. Li, S. Wang, E. Wang, Z. Han, C. Hu, N. Hu, H. Jia, *Dalton Trans.* **2003**, 233–235; b) Y. Q. Lan, X. L. Wang, K. Z. Shao, D. Y. Du, H. Y. Zang, Z. M. Su, *Inorg. Chem.* **2008**, *47*, 8179–8187; c) X. Wang, H. Lin, Y. Bi, B. Chen, G. Liu, *J. Solid State Chem.* **2008**, *181*, 556–561.

[12] a) N. M. Okun, T. M. Anderson, C. L. Hill, *J. Am. Chem. Soc.* **2003**, *125*, 3194–3195; b) B. Botar, Y. V. Geletii, P. Kögerler, D. G. Musaev, K. Morokuma, I. A. Weinstock, C. L. Hill, *J. Am. Chem. Soc.* **2006**, *128*, 11268–11277; c) Y. Nishiyama, Y. Nakagawa, N. Mizuno, *Angew. Chem. Int. Ed.* **2001**, *40*, 3639–3641; d) F. Yu, X. J. Kong, Y. Y. Zheng, Y. P. Ren, L. S. Long, R. B. Huang, L. S. Zheng, *Dalton Trans.* **2009**, 9503–9509.

[13] a) N. M. Okun, T. M. Anderson, K. I. Hardcastle, C. L. Hill, *Inorg. Chem.* **2003**, *42*, 6610–6612; b) Y. V. Geletii, B. Botar, P. Kögerler, D. A. Hillesheim, D. G. Musaev, C. L. Hill, *Angew. Chem. Int. Ed.* **2008**, *47*, 3896–3899; c) J. W. Han, C. L. Hill, *J. Am. Chem. Soc.* **2007**, *129*, 15094–15095; d) O. A. Kholdeeva, G. M. Maksimov, R. I. Maksimovskaya, M. P. Vanina, T. A. Trubitsina, D. Y. Naumov, B. A. Kolesov, N. S. Antonova, J. J. Carbo, J. M. Poblet, *Inorg. Chem.* **2006**, *45*, 7224–7234.

[14] a) S. Hasegawa, S. Horike, R. Matsuda, S. Furukawa, K. Mochizuki, Y. Kinoshita, S. Kitagawa, *J. Am. Chem. Soc.* **2007**, *129*, 2607–2614; b) J. S. Seo, D. Whang, H. Lee, S. I. Jun, J. Oh, Y. J. Jeon, K. Kim, *Nature* **2000**, *404*, 982–986; c) M. Fujita, Y. J. Kwon, S. Washizu, K. Ogura, *J. Am. Chem. Soc.* **1994**, *116*, 1151–1152; d) R. Q. Zou, H. Sakurai, Q. Xu, *Angew. Chem. Int. Ed.* **2006**, *45*, 2542–2546; e) R. Q. Zou, H. Sakurai, S. Han, R. Q. Zhong, Q. Xu, *J. Am. Chem. Soc.* **2007**, *129*, 8402–8403; f) S. Horike, M. Dincă, K. Tamaki, J. R. Long, *J. Am. Chem. Soc.* **2008**, *130*, 5854–5855; g) T. Uemura, R. Kitaura, Y. Ohta, M. Nagaoka, S. Kitagawa, *Angew. Chem. Int. Ed.* **2006**, *45*, 4112–4116; h) T. Sato, W. Mori, C. N. Kato, E. Yanaoka, T. Kuribayashi, R. Ohtera, Y. Shiraishi, *J. Catal.* **2005**, *232*, 186–198; i) C. D. Wu, A. Hu, L. Zhang, W. Lin, *J. Am. Chem. Soc.* **2005**, *127*, 8940–8941; j) M. H. Alkordi, Y. Liu, R. W. Larsen, J. F. Eubank, M. Eddaoudi, *J. Am. Chem. Soc.* **2008**, *130*, 12639–12641; k) C. Y. Sun, S. X. Liu, D. D. Liang, K. Z. Shao, Y. H. Ren, Z. M. Su, *J. Am. Chem. Soc.* **2009**, *131*, 1883–1888; l) P. Liu, C. Wang, C. Li, *J. Catal.* **2009**, *262*, 159–168; m) N. V. Maksimchuk, M. N. Timofeeva, M. S. Melgunov, A. N. Shmakov, Yu. A. Chesalov, D. N. Dybtsev, V. P. Fedin, O. A. Kholdeeva, *J. Catal.* **2008**, *257*, 315–323.

[15] X. J. Kong, Y. P. Ren, P. Q. Zheng, Y. X. Long, L. S. Long, R. B. Huang, L. S. Zheng, *Inorg. Chem.* **2006**, *45*, 10702–10711.

[16] a) G. T. Kim, T. K. Park, H. Chung, Y. T. Kim, M. H. Kwon, J. G. Choi, *Appl. Surf. Sci.* **1999**, *152*, 35–43; b) O. Y. Khyzhun, *J. Alloys Compd.* **2000**, *305*, 1–6; c) X. L. Wang, Y. H. Wang, C. W. Hu, E. B. Wang, *Mater. Lett.* **2002**, *56*, 305–311; d) L. Wang, M. Jiang, E. B. Wang, S. Y. Lian, L. Xu, Z. Li, *Mater. Lett.* **2004**, *58*, 683–687; e) J. G. Choi, L. T. Thompson, *Appl. Surf. Sci.* **1996**, *93*, 143–149.

[17] E. Burkholder, V. Golub, C. J. O'Connor, J. Zubieta, *Inorg. Chem. Commun.* **2004**, *7*, 363–366; J. Liu, J. N. Xu, Y. B. Liu, Y. K. Lu, J. F. Song, X. Zhang, X. B. Cui, J. Q. Xu, T. G. Wang, *J. Solid State Chem.* **2007**, *180*, 3456–3462; Z. H. Yi, X. B. Cui, X. Zhang, Y. Chen, J. Q. Xu, G. D. Yang, Y. B. Liu, X. Y. Yu, H. H. Yu, W. J. Duan, *Inorg. Chem. Commun.* **2007**, *10*, 1448–1452; N. Calin, S. C. Sevov, *Inorg. Chem.* **2003**, *42*, 7304–7308.

[18] L. Lisnard, A. Dolbecq, P. Mialane, J. Marrot, E. Codjovi, F. Sécheresse, *Dalton Trans.* **2005**, 3913–3920.

[19] A. L. Spek, *Acta Crystallogr., Sect. A* **1990**, *46*, C34.

[20] V. Hulea, E. Dumitriu, F. Patcas, R. Ropot, P. Graffin, P. Moreau, *Appl. Catal. A* **1998**, *170*, 169–175; M. G. Clerici, G. Bellussi, U. Romano, *J. Catal.* **1991**, *129*, 159–167.

[21] Y. Ding, Q. Gao, G. Li, H. Zhang, J. Wang, L. Yan, J. Suo, *J. Mol. Catal. A* **2004**, *218*, 161–170.

[22] S. Vetrivel, A. Pandurangan, *J. Mol. Catal. A* **2004**, *217*, 165–174.

[23] T. Radhika, S. Sugunan, *Catal. Commun.* **2007**, *8*, 150–156.

[24] a) S. S. Bhoware, S. Shylesh, K. R. Kamble, A. P. Singh, *J. Mol. Catal. A* **2006**, *255*, 123–130; b) M. S. Niasari, *J. Mol. Catal. A* **2008**, *284*, 97–107; c) T. H. Bennur, D. Srinivas, S. Sivasanker, *J. Mol. Catal. A* **2004**, *207*, 163–171; d) P. P. Toribio, J. M. Campos-Martin, J. L. G. Fierro, *J. Mol. Catal. A* **2005**, *227*, 101–105; e) S. Velusamy, T. Punniyamurthy, *Tetrahedron Lett.* **2003**, *44*, 8955–8957; f) G. Ferguson, A. N. Ajjou, *Tetrahedron Lett.* **2003**, *44*, 9139.

[25] T. Y. Lan, J. X. Chen, X. Q. Lü, Y. B. Huang, Z. S. Li, C. X. Wei, Z. C. Zhang, *Struct. Chem.* **2006**, *17*, 35–41.

[26] *XRD Pattern Processing and Identification Program*, MDI Jade 5.0, Materials Data, Inc., Livermore, CA, USA.

[27] G. M. Sheldrick, *SADABS 2.05*, University of Göttingen, Germany.

[28] *SHELXTL 6.10*, Bruker Analytical Instrumentation, Madison, WI, **2000**.

Received: May 2, 2010
Published Online: July 27, 2010

